

A NEW TEM-TYPE DEFLECTING AND CRABBING RF STRUCTURE*

J. R. Delayen^{1,2#} and H. Wang¹

¹Thomas Jefferson National Accelerator Facility, Newport News, VA 23606, U.S.A

²Old Dominion University, Norfolk, VA 23529, USA

Abstract

A new type of rf structure for the deflection and crabbing of particle bunches is introduced. It is comprised of a number of parallel TEM-resonant lines operating in opposite phase from each other. One of its main advantages is its compactness compared to conventional crabbing cavities operating in the TM_{110} mode, thus allowing low frequency designs. The properties and characteristics of this type of structure are presented.

INTRODUCTION

Rf cavities for the deflection or crabbing of particle beams have been developed for many years. Most of them are comprised of superconducting cavities operating in the TM_{110} mode [1-4] although some are room temperature structures operating in a $\lambda/4$ mode [5] or are of H -type [6]. Crabbing rf structures have been of interest for the increase of luminosity in colliders [7,8], and more recently for the generation of sub-picosecond x-ray pulses [9,10].

The concept of the parallel-bar deflecting structure introduced here is shown in Fig. 1. It consists of 2 parallel $\lambda/2$ TEM resonant lines operating in opposite phase. The voltages generated are maximum and of opposite sign in the middle of the rods and generate a transverse electric field as shown in Fig. 2. The magnetic field is null in the mid-plane containing the beam line and is maximum where the bars meet the shorting planes, as shown in Fig. 3. Thus, unlike TM_{110} structures where the deflection is produced by interaction with the magnetic field, in the parallel-bar structure, the deflection is produced by interaction with the electric field.



Figure 1: Concept of the parallel-bar deflecting structure.

* Authored by Jefferson Science Associates, LLC under U.S. DOE Contract No. DE-AC05-06OR23177. The U.S. Government retains a non-exclusive, paid-up, irrevocable, world-wide license to publish or reproduce this manuscript for U.S. Government purposes.

#delayen@jlab.org

In the absence of beam pipe apertures, and if the outer wall were made of flat planes, the deflecting π -mode would be degenerate with the accelerating 0-mode where the 2 bars are oscillating in phase. Because the π -mode has no electric or magnetic field where the beam line meets the entrance and exit walls, while the 0-mode has an electric field, the beam pipe apertures remove the degeneracy. The mode splitting is further increased by rounding all the corners as shown in Fig. 1.

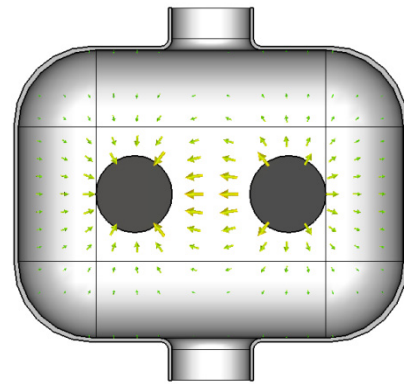


Figure 2: Electric field in the mid-plane of the parallel-bar structure operating in the π -mode.

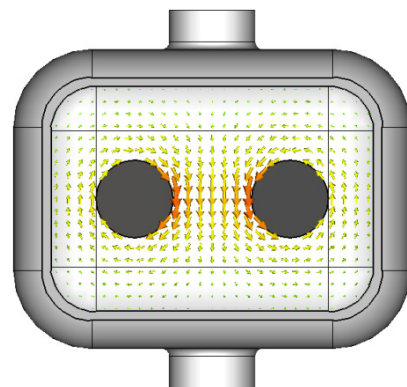


Figure 3: Magnetic field in the top-plate of the parallel-bar structure operating in the π -mode.

ANALYTICAL MODEL

If the distance between the side walls and the rods is substantially larger than the distance between the rods and the vertical symmetry plane, then the walls' contributions to the electromagnetic properties will be small and the fundamental cell can be modeled by two parallel infinite planes separated by $\lambda/2$ and joined by two parallel

cylinders of radius R and of axis-to-axis separation $2A$. The properties of such a structure can be calculated exactly, and will be compared later to simulations.

Peak Surface Electric Field

Defining the transverse electric field E_t as $E_t = 2V_t/\lambda$, where V_t is the transverse voltage acquired by an on-crest, velocity-of-light particle, the peak surface electric field E_p is

$$\frac{E_p}{E_t} = \frac{1}{4\pi} \frac{\lambda}{R} \left(\frac{\alpha+1}{\alpha-1} \right)^{1/2} \exp \left[2\pi \frac{R}{\lambda} \sqrt{\alpha^2 - 1} \right], \quad (1)$$

where $\alpha = A/R$.

Peak Surface Magnetic Field

Since this model is a uniform transmission line operating in a pure TEM mode, the peak magnetic field is related to the peak electric field by

$$B_p \text{ (in mT)} = \frac{10^9}{c} E_p \text{ (in MV/m)}. \quad (2)$$

Energy Content

The energy content U is related to the transverse gradient E_t by

$$U = E_t^2 \frac{\epsilon_0}{32\pi} \lambda^3 \cosh^{-1} \alpha \exp \left[4\pi \frac{R}{\lambda} \sqrt{\alpha^2 - 1} \right], \quad (3)$$

where ϵ_0 is the permittivity of the vacuum in SI units.

Geometrical Factor

$$G = \underline{Q}R_s = 2\pi Z_0 \frac{R}{\lambda} \frac{\cosh^{-1} \alpha}{8R \cosh^{-1} \alpha + \frac{\alpha}{\sqrt{\alpha^2 - 1}}}, \quad (4)$$

where $Z_0 = \sqrt{\mu_0/\epsilon_0} \simeq 377\Omega$ is the impedance of the vacuum.

Transverse Shunt Impedance

The transverse shunt impedance, defined as $R_t = V_t^2/P$ where P is the power dissipation, is

$$R_t/Q = 4Z_0 \frac{\exp \left[-4\pi \frac{R}{\lambda} \sqrt{\alpha^2 - 1} \right]}{\cosh^{-1} \alpha}. \quad (5)$$

It can be noted that the electromagnetic properties can be expressed simply as functions of R/λ and $\alpha = A/R$. Universal curves for the peak surface electric field and the product of the geometrical factor G and R_t/Q are shown in Figs. 4 and 5. The peak surface electric (and magnetic) field has a weak dependence on R/λ and A/R but is minimum for a rather large R/λ . G^*R_t/Q , on the other hand, has a much stronger dependence on both and is maximum for smaller R/λ . Thus the final design will depend on which parameter to optimize, and in particular whether the structure will be normal or superconducting.

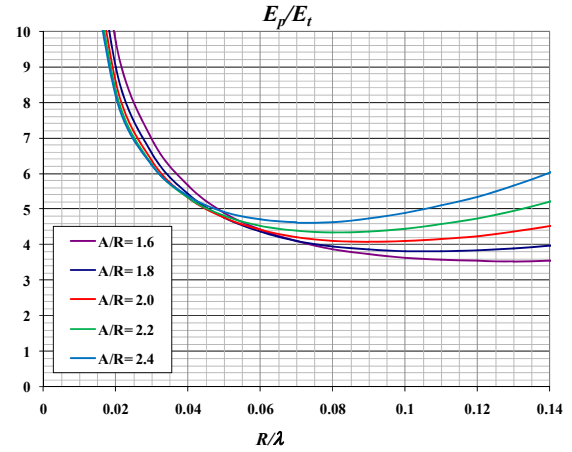


Figure 4: Ratio of peak to transverse electric field given by Eq. (1). R is the radius of the cylindrical rods and $2A$ is the distance between their axes.

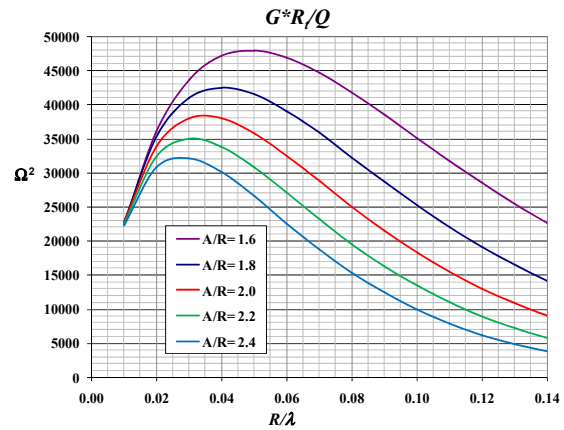


Figure 5: Product of the geometrical factor G and the transverse shunt impedance R/Q given by Eqs. (4)-(5).

ELECTROMAGNETIC DESIGN

Since one of the main characteristics of this geometry is its small transverse size, it would be particularly attractive at low frequency, and preliminary design activities have focused on a 400 MHz single-cell cavity.

The lengths of the bars and of the outer box were, to first order, fixed at 375mm and the main design parameters were the radii and separation of the two parallel bars. Results of simulations using CST Microwave Studio® are shown in Fig. 6. They compare very favorably with the analytical results of the previous section. As was expected the transverse shunt impedance of this design is quite high compared to designs based on TM_{110} modes. This is similar to the high shunt impedance of TEM accelerating structures compared to TM_{010} structures [11].

For velocity-of-light applications TEM accelerating structures have peak surface fields larger than TM_{010} structures [11]. The analytical model and these simulations show that this is not the case for deflecting cavities as peak surface fields for TEM structures are comparable to those in TM_{110} structures.

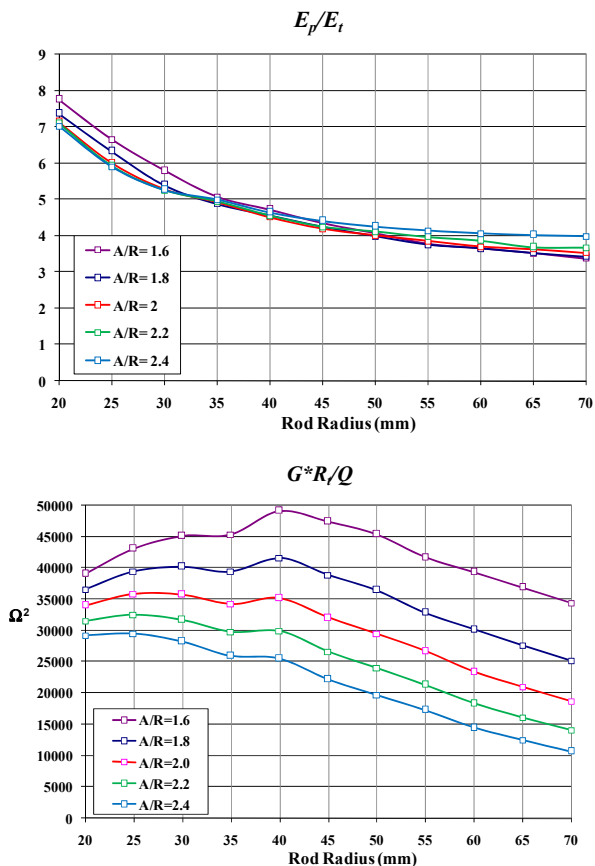


Figure 6: Ratio of peak to deflecting electric field (upper) and $G \cdot R_t / Q$ (lower) for the 400 MHz structure shown in Fig. 1 obtained from CST Microwave Studio.

Properties of a preliminary design of a 400 MHz parallel-bar deflecting structure obtained from Omega3P are shown in Table 1. It can be noted that the deflecting π -mode is the lowest frequency mode, which would simplify the damping of all the other modes in high-current applications.

EXTENSIONS AND OPTIMIZATION

The single-cell parallel bar structure discussed so far can be straightforwardly extended to a multicell structure by the addition of sets of parallel bars separated by $\lambda/2$ as shown in Fig. 7. In the relevant (deflecting) mode of operation each set of bars oscillates in opposite phase from its neighbors and each bar oscillates in opposite phase from the bar across the beam line. This will increase the degree of degeneracy since the number of TEM modes is equal to the number of bars, and splitting the (π, π) deflecting mode from all the others will need to be provided, for example by shaping the outer walls or introducing partial walls between the sets of bars.

All the above examples use straight circular cylinders for the bars. Further optimization can be obtained by deviation from a circular cross-section, deviation from a constant cross-section (hyperboloidal shape), deviation from a straight bar centerline. These modifications could

yield geometries with lower surface magnetic field, for example, at the expense of added engineering complexity.

Table 1: Properties of Parallel-bar Structure shown in Figure 1 Calculated from Omega3P and Analytical Model

Parameter	Ω3P	Analytical model	Unit
Frequency of π -mode	400	400	MHz
$\lambda/2$ of π -mode	374.7	374.7	mm
Frequency of 0-mode	414.4	400	MHz
Cavity length	374.7	∞	mm
Cavity width	500	∞	mm
Bars length	381.9	374.7	mm
Bars diameter ($2R$)	100	100	mm
Bars axes separation ($2A$)	200	200	mm
Aperture diameter	100	0	mm
Deflecting voltage V_t^*	0.375	0.375	MV
E_p^*	4.09	4.28	MV/m
B_p^*	13.31	14.25	mT
U^*	0.215	0.209	J
G	96.0	112	Ω
R_t/Q	260	268	Ω

* at $E_t=1\text{MV/m}$

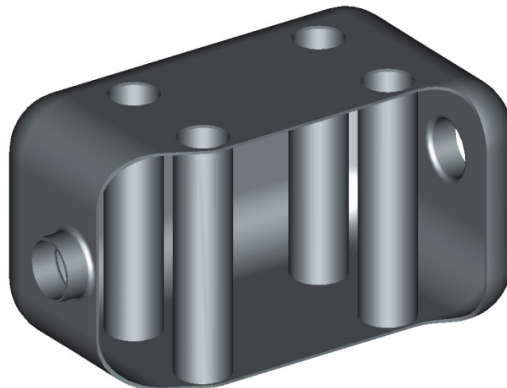


Figure 7: Concept for a 2-cell parallel-bar deflecting cavity. Each of the bars oscillates in opposite phase from its two nearest neighbors.

REFERENCES

- [1] A. Citron *et al.*, NIM **155** (1978), p. 93.
- [2] H. Padamsee *et al.*, Proc. PAC91, p. 2423.
- [3] K. Hosoyama *et al.*, Proc. APAC98, p. 828.
- [4] T. W. Koeth, Proc. PAC99, p. 995.
- [5] C. W. Leemann and C. G. Yao, Proc. LINAC90, p. 232.
- [6] Yu. Senichev *et al.*, PRSTAB **9**, 012001 (2006).
- [7] R. B. Palmer, SLAC-PUB 4707 (1988).
- [8] K. Oide and K. Yokoya, Phys. Rev. **A40**, p. 315 (1989).
- [9] A. Zholents, P. Heimann, M. Zolotarev, and J. Byrd, NIM **A425**, 385 (1999)
- [10] J. Shi *et al.*, Proc. PAC05, p. 4287.
- [11] J. R. Delayen, Proc. 2001 SRF Workshop, p. 152.